Preprints.org

Article

Not peer-reviewed version

Simulation Study on the Mechanical Properties of Fuzz Button

Xiuping Dong , Zhongping Zhang , Mingji Huang *

Posted Date: 25 May 2026

doi: 10.20944/preprints202605.1563.v1

Keywords: fuzz button; microstructure model; simulation method; mechanical performance; damping and energy dissipation

Preprints.org is a free multidisciplinary platform providing preprint service that is dedicated to making early versions of research outputs permanently available and citable. Preprints posted at Preprints.org appear in Web of Science, Crossref, Google Scholar, Scilit, Europe PMC, OpenAlex.

Copyright: This open access article is published under a Creative Commons CC BY 4.0 license, which permit the free download, distribution, and reuse, provided that the author and preprint are cited in any reuse.

Preprints.org (www.preprints.org) | NOT PEER-REVIEWED | Posted: 25 May 2026 doi:10.20944/preprints202605.1563.v1

Disclaimer/Publisher's Note: The statements, opinions, and data contained in all publications are solely those of the individual author(s) and contributor(s) and not of MDPI and/or the editor(s). MDPI and/or the editor(s) disclaim responsibility for any injury to people or property resulting from any ideas, methods, instructions, or products referred to in the content.

Article

Simulation Study on the Mechanical Properties of Fuzz Button

Xiuping Dong [1], Zhongping Zhang [1] and Mingji Huang [2,*]

[1] University of Technology and Business Beijing, Beijing 100048, China

[2] University of Science and Technology Beijing, Beijing 100083, China

* Correspondence: huangmingji@ustb.edu.cn

Abstract

As a novel solderless vertical interconnection structure, the fuzz button exhibits broad application prospects in high-density electronic packaging and high-reliability interconnection systems owing to its low profile, separable interconnection capability, and excellent environmental adaptability. However, due to its complex internal geometric configuration and contact nonlinearity, conventional equivalent modeling approaches are insufficient to accurately characterize its actual mesoscopic structure and mechanical behavior. To address this issue, a finite element simulation method for fuzz buttons based on virtual fabrication was proposed. A trajectory generation method describing the "movement–direction change–fixation–reset" process of metallic wires was first established based on a three-dimensional braiding technique, and cubic spline interpolation was employed to smooth and fit the trajectories, thereby constructing a three-dimensional preform model of the fuzz button. Subsequently, the compression molding process was implemented in Abaqus to obtain a fuzz button model possessing realistic geometric morphology and mesoscopic contact topology characteristics. Considering the pronounced contact nonlinearity and large deformation behavior, the penalty function method was adopted to handle the complex contact interactions among metallic wires, while an explicit dynamic solver with displacement-controlled loading was employed for numerical computation. The mesh was discretized using C3D8R solid elements, and local mesh refinement was introduced in the contact regions to balance computational accuracy and efficiency. Key mechanical response data, including reaction force–displacement curves and energy dissipation characteristics, were extracted and validated experimentally. The results demonstrate that the proposed finite element simulation method can effectively reproduce the compressive behavior and nonlinear hysteretic response of fuzz buttons, with good agreement achieved between simulation and experimental results. The proposed approach provides an effective tool and theoretical basis for mesoscopic structural modeling, mechanical performance analysis, and structural optimization design of fuzz button contacts.

Keywords: fuzz button; microstructure model; simulation method; mechanical performance; damping and energy dissipation

1. Introduction

With the continuous evolution of electronic packaging technologies toward miniaturization, high-density integration, and high reliability, micro-interconnection structures are increasingly subjected to severe electro–thermal–mechanical multiphysics coupling challenges under complex service environments [1–3]. As a novel solderless vertical interconnection unit, the fuzz button demonstrates significant application potential in aerospace electronics, high-density PCB assembly, automotive electronics, and high-frequency communication modules due to its low profile, separable interconnection capability, short transmission path, and superior comprehensive electro–thermal–mechanical performance [4–7]. The principle of vertical interconnection is illustrated in Figure 1. Compared with conventional radio-frequency connectors and flip-chip bonding technologies, fuzz

© 2026 by the author(s). Distributed under a Creative Commons CC BY license.

Preprints.org (www.preprints.org) | NOT PEER-REVIEWED | Posted: 25 May 2026 doi:10.20944/preprints202605.1563.v1

buttons form conductive pathways through the entanglement of internal metallic wires, thereby effectively shortening signal transmission distances and reducing reliability risks associated with solder joint fatigue failure and interface misalignment [8–10]. Therefore, establishing a high-fidelity model capable of accurately representing the internal mesoscopic structure of fuzz buttons and investigating their mechanical behavior on this basis are of considerable theoretical significance and engineering value for the reliable application of such interconnection structures.

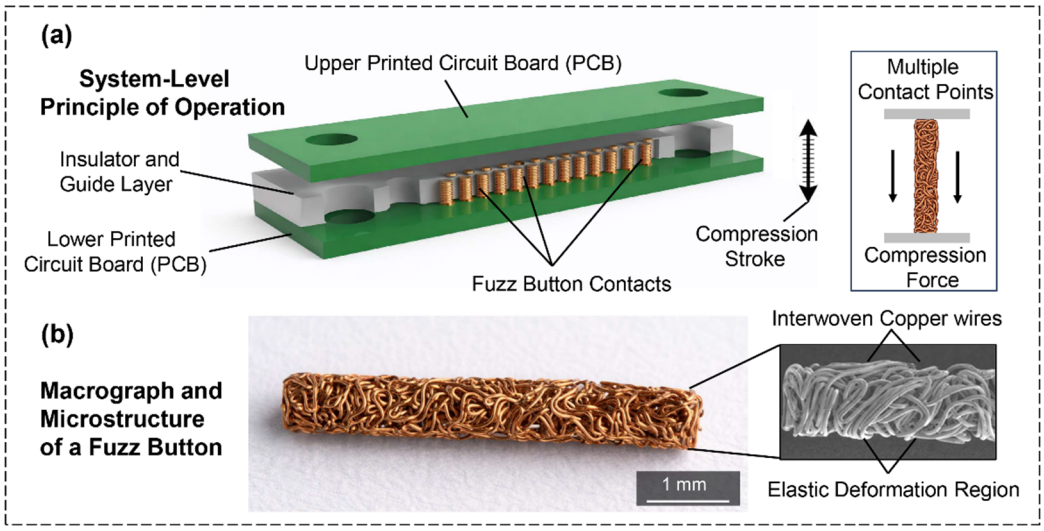

Figure 1. Schematic illustration of fuzz button vertical interconnection and high-magnification macroscopic image of the physical specimen.

Existing studies on the mechanical and electrical properties of fuzz buttons have mainly focused on experimental characterization and theoretical modeling. In terms of experimental investigations, Harris et al. [11] systematically evaluated the force–displacement behavior and contact resistance evolution of fuzz button contacts fabricated from different materials during compression. Their results indicated that the electrical resistance decreased rapidly with increasing compression displacement and gradually stabilized; however, the inherent randomness of the wire entanglement process resulted in significant dispersion in the mechanical responses among different specimens. Lv et al. [12] further investigated the rebound behavior of fuzz buttons fabricated from different materials under cyclic compression conditions from the perspective of intrinsic wire properties, revealing the critical influence of material mechanical properties on rebound stability. These studies provided fundamental experimental support for material selection and mechanical performance evaluation of fuzz buttons.

At the theoretical modeling level, researchers have attempted to correlate the complex internal structure of fuzz buttons with their macroscopic mechanical responses using equivalent modeling approaches. Huang et al. [13] simplified the random metallic wire network into polyline beam elements and established a macroscopic constitutive model of the fuzz button based on an equivalent spring network, thereby investigating the effects of wire diameter, elastic modulus, relative density, and geometric parameters on the overall compressive response. Zhu et al. [14] adopted an equivalent homogenization approach to establish a finite element model of a fuzz button connector assembly and analyzed load transfer, stress distribution, and structural response under impact loading conditions during compression. In addition, Zhang et al. [15] developed electrical simulation models with different hierarchical levels based on the actual fuzz button configuration and verified their effectiveness in predicting electrical performance. Lall et al. [16] established a numerical model to investigate contact surface wear behavior, while Zhu et al. [17] compared the rebound performance of fuzz buttons fabricated from different materials through simulation analysis. Zhang et al. [18] proposed a finite element modeling method based on digital manufacturing technology, enabling

© 2026 by the author(s). Distributed under a Creative Commons CC BY license.

Preprints.org (www.preprints.org) | NOT PEER-REVIEWED | Posted: 25 May 2026 doi:10.20944/preprints202605.1563.v1

full-process simulation from wire-entangled preform generation to compression molding. Although these studies have advanced the structural design and engineering application of fuzz buttons from various perspectives, equivalent homogenization approaches and simplified idealized geometric models remain insufficient for accurately characterizing the inherently porous, disordered, and interwoven mesoscopic topological features of fuzz buttons. Significant limitations still exist in describing critical mechanical behaviors, including contact nonlinearity, large deformation, and local plastic evolution.

Although preliminary studies have explored modeling approaches based on realistic mesoscopic geometries, limited research has been conducted on finite element solution strategies for such extremely complex porous network structures. The interior of a fuzz button contains a massive number of randomly distributed spatial metallic wire contact pairs, which undergo strongly nonlinear evolution from point contact and relative sliding to localized severe extrusion during loading and unloading processes. Existing simulation studies have primarily focused on the output of macroscopic responses or idealized structural representations, whereas investigations on full-cycle numerical simulation strategies encompassing preprocessing, solver configuration, and postprocessing remain insufficient. The oversimplified treatment of the underlying solution mechanisms often leads to computational bottlenecks under large compression strokes, including contact penetration, mesh distortion, and convergence difficulties.

To address the aforementioned technical limitations, a finite element numerical simulation method for fuzz buttons based on virtual fabrication was proposed in this study, in which the critical stages throughout the entire simulation cycle were systematically optimized. A refined contact constraint strategy was established to accurately characterize the complex spatial contact states among metallic wires. Considering the complexity of the internal spatial topology, a local optimization strategy was introduced to balance high-resolution contact boundary solutions with computational convergence efficiency. Furthermore, a comprehensive quantitative analysis framework was developed for evaluating force–displacement hysteretic responses and energy dissipation characteristics. Combined with quasi-static compression experiments for validation, the proposed method can effectively reveal the mesoscopic mechanisms underlying the nonlinear hysteretic behavior of fuzz buttons and provide robust and efficient simulation support for high-fidelity mechanical prediction of related complex micro-interconnection structures.

2. Virtual Fabrication of Fuzz Buttons

2.1. Principle of Preform Trajectory Generation

The internal structure of a fuzz button contact is formed by the mutual entanglement, stacking, and subsequent compression molding of fine metallic wires in three-dimensional space, resulting in a mesoscopic structure characterized by significant porosity, randomness, and complex contact features [19–21]. Owing to the disordered arrangement and complex geometric morphology of metallic wires inside actual fuzz buttons, it is difficult to directly establish a finite element model with realistic topological characteristics. Therefore, combined with the actual fabrication process of fuzz buttons, a virtual fabrication strategy was adopted to digitally reconstruct both the preform structure and the forming process. In practical manufacturing, the fabrication of fuzz buttons generally includes metallic wire pretreatment, wire entanglement forming, compression molding, and subsequent heat treatment processes [22]. The essence of the preform structure lies in the continuous spatial braiding and interlaced accumulation of metallic wires. Accordingly, a three-dimensional braiding “four-step method” was introduced to parametrically describe the trajectories of metallic wires. The core concept of this method is to arrange metallic wires spatially according to prescribed rules and impose periodic motions along the X-, Y-, and Z-directions [23–25]. A complete braiding cycle sequentially consists of row-wise movement, column-wise movement, reverse row-wise movement, and reverse column-wise movement, through which the metallic wires gradually form

© 2026 by the author(s). Distributed under a Creative Commons CC BY license.

Preprints.org (www.preprints.org) | NOT PEER-REVIEWED | Posted: 25 May 2026 doi:10.20944/preprints202605.1563.v1

an integrated three-dimensional porous network structure. The principle of the three-dimensional braiding four-step method is illustrated in Figure 2.

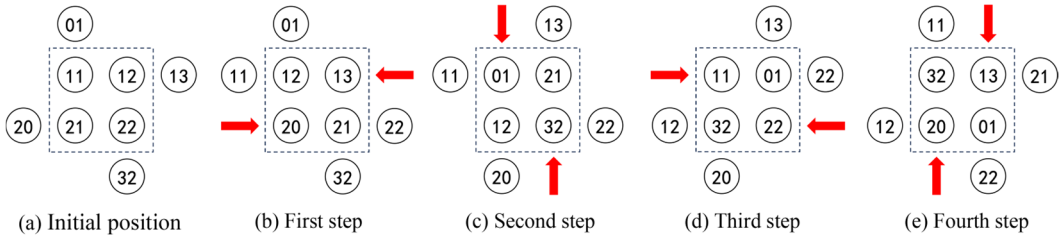

Figure 2. Process Diagram of the Four-Step Braiding Method for 3D Models.

The proposed method does not assume the internal solid morphology of the fuzz button in advance; rather, it derives the preform structure from the spatial motion of metallic wires, transforming the generation of the preform into a trajectory evolution problem. By adjusting parameters such as braiding step length, motion direction, and the number of cycles, the external dimensions, internal pore distribution, and overall density of the preform can be controlled, yielding a model with a clear geometric origin and parametrizable features suitable for subsequent finite element analysis.

The spatial motion of metallic wires during the braiding process is categorized into four fundamental behaviors—motion, direction change, fixation, and reset—to construct the central trajectory. These four behaviors act synergistically within a single braiding cycle to drive the continuous evolution of the wires. Table 1 summarizes the complete steps of one braiding cycle in the four-step method.

Table 1. Four-Step Method – Periodic Braiding Steps.

Step	Direction of Motion	Even Rows/Columns	Odd Rows/Columns	Z Direction
1	Along X direction	(x-1, y, z+1) - move left	(x+1, y, z+1) - move right	Z+1
2	Along Y direction	(x, y-1, z+1) - move up	(x, y+1, z+1) - move down	Z+1
3	Along X direction (reverse)	(x+1, y, z+1) - move right	(x-1, y, z+1) - move left	Z+1
4	Along Y direction (reverse)	(x, y+1, z+1) - move down	(x, y-1, z+1) - move up	Z+1

The motion behavior describes the continuous extension of the wire along a prescribed direction in space and constitutes the primary mechanism for forming the basic preform skeleton. This behavior is determined jointly by the direction of motion and the step length. Motion in the X and Y directions governs the planar distribution and winding pattern of the wire, while motion in the Z direction controls the interlayer stacking along the thickness. By setting the step lengths in each direction, preliminary control over the preform dimensions and porosity can be achieved.

The direction-change behavior is activated when a metallic wire reaches a preset boundary, redistributing its motion direction so that planar extension ceases and interlayer transitions along the thickness direction are completed. This behavior ensures that the trajectories form a uniform and symmetric distribution in space, preventing local structural looseness and providing a stable initial geometric basis for subsequent compression molding.

After the local trajectory of a wire is generated, fixation behavior is applied to enhance the overall stability of the preform structure by establishing connections between adjacent trajectories. Fixation includes two forms: intra-layer adjacent fixation and interlayer connection fixation. The former

© 2026 by the author(s). Distributed under a Creative Commons CC BY license.

Preprints.org (www.preprints.org) | NOT PEER-REVIEWED | Posted: 25 May 2026 doi:10.20944/preprints202605.1563.v1

creates a relatively stable planar support within each layer, while the latter enables load transfer between layers. Together, they construct a complete three-dimensional network topology, transforming the preform from a simple collection of trajectories into an integrated spatially braided structure.

Upon completing a braiding cycle, the wire trajectories are returned to a new initial state for the next cycle, a process defined as the reset behavior. This behavior ensures the periodicity of trajectory evolution, allowing a single metallic wire to continuously extend according to the same rules while imparting a macroscopically uniform, repetitive stacking feature to the preform structure. By adjusting the number of cycles and the Z-direction step length, the overall height and internal layer distribution of the preform can be further controlled.

Through the continuous interaction of these four behaviors, discrete spatial trajectory points for each metallic wire in the fuzz button preform can be generated.

2.2. Three-Dimensional Preform Modeling

Directly connecting the discrete trajectory points can easily produce geometric sharp corners and local discontinuities, which adversely affect the accuracy and convergence of subsequent contact analysis. To address this issue, cubic spline interpolation was employed to smoothly fit the trajectory of each metallic wire, yielding continuous and smooth spatial curves [26–28], as shown in Figure 3a. Based on this, the fitted trajectory coordinate data were imported into the SolidWorks environment via the SolidWorks API interface. In SolidWorks, the discrete trajectory points were connected using smooth curves to create the preform sketches. Subsequently, each wire trajectory curve was swept with the metallic wire radius as the sweeping parameter, producing the three-dimensional preform model of the fuzz button, as illustrated in Figure 3b.

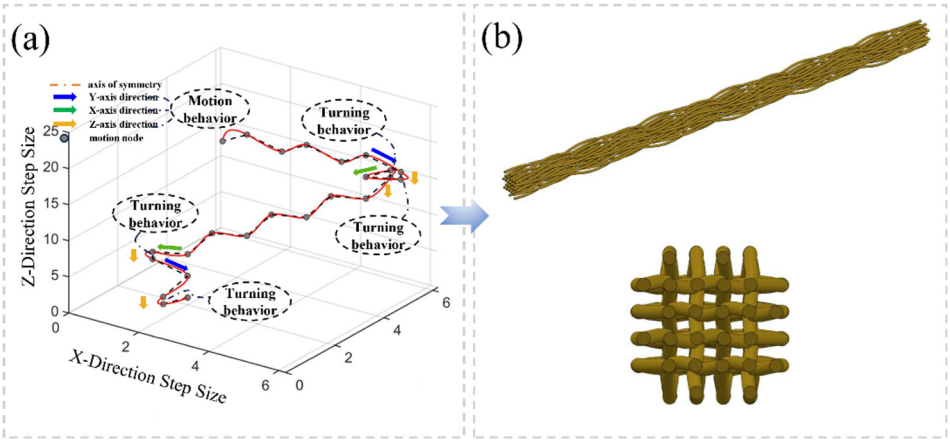

Figure 3. Generation process of fuzz button preform: (**a**) Preform trajectory coordinates; (**b**) Three-dimensional preform model.

2.3. Three-Dimensional Modeling of Fuzz Buttons

The constructed preform model reflects only the initial configuration of the metallic wires during the braiding stage and cannot be directly used as a finite element model of the fuzz button in its service state. In the actual fabrication process, the preform undergoes compression molding, experiencing significant axial compression, radial expansion, and internal contact reorganization under external forces. Therefore, it is necessary to further geometrically refine the preform and reconstruct its contact state through a virtual compression process.

Virtual compression modeling first requires the construction of a stamping die. The target diameter of the fuzz button was used as the design basis for the inner diameter of the cylindrical die cavity, while the die wall thickness and outer diameter were determined by considering machining accuracy and structural rigidity requirements [29,30]. The die height was modeled in segments

© 2026 by the author(s). Distributed under a Creative Commons CC BY license.

Preprints.org (www.preprints.org) | NOT PEER-REVIEWED | Posted: 25 May 2026 doi:10.20944/preprints202605.1563.v1

according to the preform height and punch stroke, and the bottom structure was refined to finalize the three-dimensional cylindrical die model.

Based on this, an assembly of punch–preform–die was established in Abaqus. The metallic wires of the preform were defined as deformable bodies, while the punch and die were treated as rigid boundary components. Axial compression of the preform was driven by displacement-controlled motion of the punch. Following a prescribed time–displacement history, the loading, holding, and unloading stages were sequentially simulated, representing the entire process of the fuzz button transitioning from a loose preform to a densified molded component, as illustrated in Figure 4a. After compression, elastic recovery of the preform produced a certain amount of springback, resulting in a final geometry that closely matches the physical fuzz button in both external dimensions and internal structural features, as shown in Figure 4b.

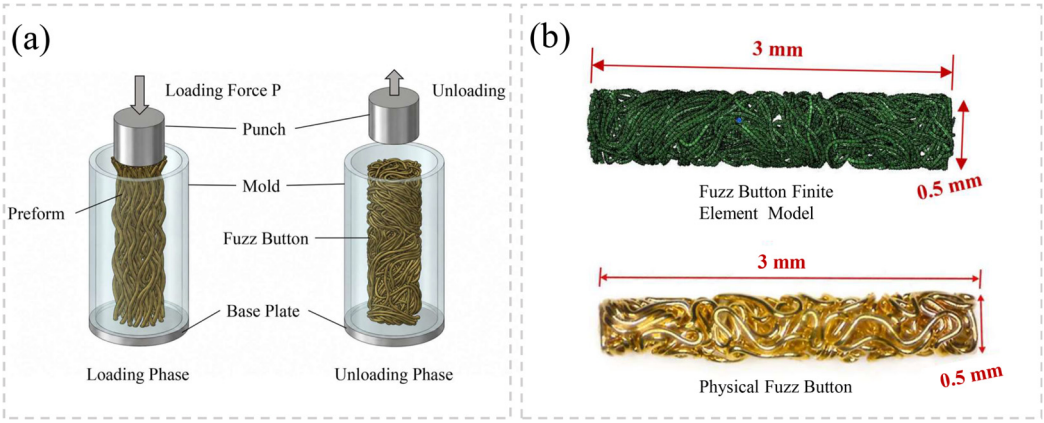

Figure 4. Numerical modeling of the fuzz button forming process: (**a**) Schematic of compression; (**b**) Comparison between fuzz button model and physical specimen.

3. Fuzz Button Finite Element Simulation Method

3.1. Finite Element Preprocessing

The three-dimensional mesoscopic model of the fuzz button was imported, and an assembly of punch–fuzz button–die was established in Abaqus. The fuzz button consists of multiple solid metallic wires, retaining the realistic spatial entanglement and initial contact topology among the wires. The punch is positioned above the fuzz button, while the die is located below, together forming the basic assembly for compression analysis. Considering that the primary deformation of the fuzz button during compression is concentrated within the internal wire network and that the punch and die possess high rigidity with negligible deformation, the punch and die were simplified as rigid bodies, while only the fuzz button was defined as a deformable body. This treatment reduces the model's degrees of freedom, improves computational efficiency, and focuses the analysis on the stress and deformation behavior of the fuzz button's complex internal structure while maintaining simulation accuracy.

Beryllium copper (BeCu) alloy, a common material for fuzz buttons, was used as the baseline material for the finite element model, with corresponding material properties assigned. The material parameters of the metallic wires include the elastic modulus, density, and Poisson's ratio, with an elastic modulus of 1.28×10^5 MPa, a Poisson's ratio of 0.3, and a density of 8.25 g/mm^3. The material property settings of the model are summarized in Table 2.

Table 2. Material Property Settings.

Density (g/mm^3)	Young's Modulus (GPa)	Poisson's Ratio	Bulk Modulus (GPa)	Shear Modulus (GPa)
8.25	128	0.3	106.7	49.2

© 2026 by the author(s). Distributed under a Creative Commons CC BY license.

Preprints.org (www.preprints.org) | NOT PEER-REVIEWED | Posted: 25 May 2026 doi:10.20944/preprints202605.1563.v1

During compression, the metallic wires within the fuzz button undergo not only bending-induced yielding and contact extrusion but also irreversible plastic deformation. When the wire diameter is reduced to the order of tens of micrometers, the number of internal grains decreases significantly, and conventional macroscopic continuum mechanics models fail to accurately capture the mechanical response. In this regime, the material exhibits a pronounced size effect in which the yield strength increases as the characteristic dimension decreases ("smaller is stronger") [31–33]. To reasonably incorporate such microscale effects into the simulation, a correction method based on strain gradient plasticity theory was adopted [34–36]. Considering that the forming and compression processes of fuzz buttons involve numerous microscale bending regions, directly solving higher-order strain gradient equations would substantially increase computational cost and lead to convergence difficulties. Therefore, an equivalent strategy was employed in which the material constitutive curve is directly corrected, embedding the microscale effects into the finite element model without additional computational burden and thereby improving the prediction accuracy of forming springback.

The plastic strain data were corrected according to the Nix–Gao strain gradient plasticity theory [37], using the following Equations (1) and (2):

$$l^* = \frac{M^2 \alpha^2 G^2 b}{\sigma_0^2} \tag{1}$$

$$K = \sqrt{1 + \frac{l^*}{R_{bend}}} \tag{2}$$

where l^* is the characteristic intrinsic length, R_{bend} is the characteristic bending radius, and K is the stress correction amplification factor.

For beryllium copper alloy, the characteristic intrinsic length l^* is typically 0.003 mm. For a fuzz button with a wire diameter of 0.08 mm, assuming the wire is fully compressed within the die, the characteristic bending radius is approximately half of the wire diameter, i.e., R_{bend} is 0.04 mm. Accordingly, the calculated correction amplification factor is K = 1.0368. The corrected yield stress–plastic strain curve is presented in Figure 5.

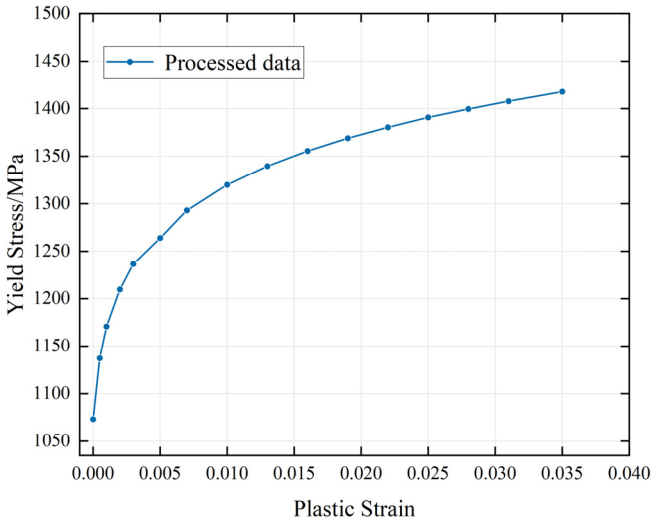

Figure 5. Corrected stress-strain curve.

During compression, the metallic wires within the fuzz button undergo not only overall bending deformation but also localized contact extrusion, plastic evolution, and multiple random contact points. Therefore, solid elements suitable for complex contact and large deformation problems are required for discretization. In this study, the metallic wires were meshed using eight-node linear reduced integration three-dimensional solid elements (C3D8R) in Abaqus. These elements employ a reduced integration scheme that balances computational efficiency with solution accuracy, effectively

© 2026 by the author(s). Distributed under a Creative Commons CC BY license.

Preprints.org (www.preprints.org) | NOT PEER-REVIEWED | Posted: 25 May 2026 doi:10.20944/preprints202605.1563.v1

lowering the computational cost of large-scale contact analysis while demonstrating good compatibility with explicit dynamic solvers, making them suitable for handling the highly nonlinear behavior of the fuzz button mesoscopic model [38]. The punch and die were simplified as rigid bodies with negligible deformation; thus, they could be discretized using coarser meshes or analytical rigid body representations, as they are not the primary focus of deformation analysis. Through mesh convergence analysis, the global mesh size of the fuzz button preform was determined to be 0.015 mm, ensuring computational accuracy while controlling the model size and avoiding element penetration or collapse during compression. The element types and quantities for each component are summarized in Table 3, with the punch meshed using C3D8R elements and the die using C3D10M elements.

Table 3. Number and types of elements for each component.

Item	Braided button preform	Punch	Die
Total number of elements	60108	3520	15997
Element type	C3D8R	C3D8R	C3D10M
Approximate global size / mm	0.052	0.25	0.25
Maximum deviation factor	0.1	0.1	0.1
Element order	First order	First order	First order
Mesh type	Hexahedron	Hexahedron	Tetrahedron

During compression, the fuzz button involves complex multipoint contact interactions, relative sliding, and localized extrusion not only among metallic wires but also between the wires and the punch and die. Therefore, the proper definition of contact relationships is critical for finite element simulation. Accordingly, contact pairs were established for wire–wire, wire–punch, and wire–die interactions to simulate the dynamic evolution of contact states during compression and unloading.

The normal contact behavior was treated using the penalty function method, in which the penetration between contact nodes is controlled through the introduction of contact stiffness. The penalty method exhibits good numerical stability and is particularly suitable for solving the large number of random contact pairs present within the fuzz button structure. The tangential behavior was described using the Coulomb friction model, where the friction coefficient characterizes the relative sliding and frictional damping effects between metallic wires.

For three-dimensional contact problems, the contact interfaces exhibit strong nonlinearity, and the governing equations consist of the coupling between equilibrium equations and contact constraints. The virtual work equation with contact constraints can be expressed as follows [39]:

$$G(u_t, u_\delta) - \int_{\Gamma_c} P_c^t \times u_\delta d\Gamma_c^t = 0 \tag{3}$$

Where $G(u_t, u_\delta) = \int_\Omega \sigma_t : grad(u_\delta) d\Omega_t - \int_\Omega F_t \times u_\delta d\Omega_t - \int_{\Gamma_s} T_t \times u_\delta d\Gamma_s^t$, Γ_s^t denotes the boundary condition subjected to external forces, and Γ_c^t represents the boundary of the potential contact region. "Grad" denotes the gradient operator, and Ω_t represents the contact system, while σ_t, F_t, T_t, and P_c^t denote the stress, body force, surface traction, and contact force, respectively. Consistent with the equilibrium conditions on the stress boundary, the contact penetration at the contact point $X \in \Gamma_c$ can be determined through Equation (3). On this basis, the relationship between the contact force and the contact displacement increment was established by combining the penalty function method with non-classical friction theory.

The nodal contact penetration at each load step can be determined using Equation 3. On this basis, the relationship between the contact force and the contact displacement increment was established by incorporating the penalty function and non-classical friction theory:

© 2026 by the author(s). Distributed under a Creative Commons CC BY license.

Preprints.org (www.preprints.org) | NOT PEER-REVIEWED | Posted: 25 May 2026 doi:10.20944/preprints202605.1563.v1

$$dP_c = E_{ct} dg_c \tag{4}$$

$$E_{ct} = \begin{bmatrix} \varepsilon_T \left(1 - \omega \frac{P_{T1}^2}{|P_T|^2}\right) & -\omega \varepsilon_T \frac{P_{T1} P_{T2}}{|P_T|^2} & \omega \mu \varepsilon_N \frac{P_{T1}}{|P_T|} \\ -\omega \varepsilon_T \frac{P_{T1} P_{T2}}{|P_T|^2} & \varepsilon_T \left(1 - \omega \frac{P_{T2}^2}{|P_T|^2}\right) & \omega \mu \varepsilon_N \frac{P_{T2}}{|P_T|} \\ 0 & 0 & \varepsilon_N \end{bmatrix} \tag{5}$$

where ω denotes the contact-state factor, with ω = 0 corresponding to sticking contact and ω = 1 corresponding to the sliding state.

Based on the above contact-mechanics framework, the contact parameters of the fuzz button model were calibrated. Normal contact was implemented using the penalty function method, with the stiffness scaling factor set to 0.8. Numerical verification showed that, under this setting, the maximum penetration between metallic wires was less than 1% of the characteristic mesh size, thereby satisfying engineering accuracy requirements while avoiding solution oscillations caused by excessive contact stiffness. The tangential friction coefficient was set to 0.12 according to the dry, unlubricated surface characteristics of beryllium copper alloy. This value determines the critical shear-stress threshold for the transition between sticking and sliding states in the contact stiffness matrix E_{ct} in Equation 5. It can be inferred from the matrix structure of Equation 5 that the switching of the contact state exhibits pronounced nonlinear characteristics. For the large number of contact pairs inside the fuzz button, directly imposing contact constraints using the Lagrange multiplier method would lead to a sharp increase in the dimensionality of the system stiffness matrix and would readily induce saddle-point problems. By allowing a negligible amount of penetration, the penalty function method effectively ensures the numerical stability of large-scale random contact analyses and is therefore more suitable for the contact solution of the present model. The complete contact parameter settings are summarized in Table 4. The above contact definition can effectively capture the contact evolution characteristics of metallic wires inside the fuzz button during loading, progressing from localized point contact and sliding contact in the initial stage to compressive contact and localized sticking states in the middle and later stages.

Table 4. Contact Property Settings.

Contact Property	Friction Coefficient	Pressure Interference	Friction Formulation
Tangential Behavior	0.12	/	Penalty function
Normal Behavior	/	Hard contact	/

3.2. Analysis Step and Solver Settings

During the compression forming of the fuzz button, the metallic wires continuously deform and displace under the applied load, causing the contact positions between the wires and the die surface, as well as the contact states among the wires, to evolve continuously throughout the loading process. This constitutes a typical contact nonlinearity problem [40]. When applied to such large-scale random contact problems, static implicit solution methods often suffer from convergence difficulties or local solution failures due to abrupt switching of contact states. Therefore, an explicit dynamic solver was employed to simulate the compression process. Explicit dynamics performs time integration based on the central difference method and does not require iterative solution of the tangent stiffness matrix, enabling stable treatment of highly nonlinear contact and complex large-deformation problems [41].

Owing to the high degree of nonlinearity of the model, direct use of explicit dynamic analysis would result in excessively small time increments and frequent increment reductions. Therefore, a quasi-static analysis strategy was adopted. To accurately characterize the quasi-static compression behavior, the loading rate must be strictly controlled and appropriate mass scaling must be introduced to ensure that the kinetic energy of the system remains below 5% of the internal energy,

© 2026 by the author(s). Distributed under a Creative Commons CC BY license.

Preprints.org (www.preprints.org) | NOT PEER-REVIEWED | Posted: 25 May 2026 doi:10.20944/preprints202605.1563.v1

thereby eliminating the influence of inertial effects. The analysis step settings are listed in Table 5. The entire loading process was divided into loading and unloading stages according to the time–displacement amplitude curve, corresponding to the gradual compression of the fuzz button by the punch and the elastic recovery after punch removal, respectively. Smooth displacement amplitude functions were adopted in both stages to suppress dynamic oscillations induced by impact loading and to improve the accuracy of the quasi-static solution.

Table 5. Analysis Settings.

Analysis Step	Geometric Nonlinearity	Time Period	Natural Frequency	Increment Step
Loading	Yes	1	100	1e-5
Unloading	Yes	1	100	1e-5

In terms of boundary conditions, the bottom of the die was fully constrained, with all translational and rotational degrees of freedom restricted. The punch was allowed to retain only the displacement degree of freedom along the compression direction (Z direction), while the remaining degrees of freedom were constrained. The bottom surface of the fuzz button was in contact with the die, whereas its upper surface was in contact with the punch, thereby establishing a complete axial compression path. The load was applied through a prescribed displacement history of the punch along the Z direction. The total loading displacement was set to 0.8 mm, and a staged displacement history was employed to complete the entire loading and unloading process, thereby approximating the actual compression conditions of the fuzz button.

3.3. Post-Processing Method

In the post-processing stage, the displacement field, equivalent stress field, and equivalent plastic strain field during the entire compression process of the fuzz button were extracted. In addition, the evolution of the contact state among metallic wires was tracked in representative local regions, as shown in Figure 6. By comparing the distributions of field variables at different loading stages, the micromechanical response mechanism of the internal metallic wires during compression can be revealed. In particular, in the wire crossing and bending regions, the local contact normal pressure gradually increases with increasing compression displacement, and the contact mode progressively evolves from initial point contact and local sliding to compressive contact and local sticking, thereby inducing stress concentration and plastic strain accumulation.

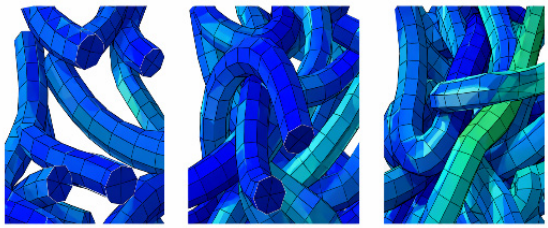

Figure 6. Evolution of contact state.

To obtain the macroscopic mechanical response of the fuzz button, the displacement and reaction force data of the punch reference point were extracted throughout the loading–unloading process to construct the force–displacement hysteresis curve. This curve can directly characterize the load-bearing capacity, nonlinear stiffness variation, and hysteretic energy dissipation characteristics of the fuzz button. During data processing, the curve was divided into loading and unloading segments according to its variation trend, and baseline correction was performed on the original response. Nonphysical negative values near zero were truncated to zero to reduce the influence of numerical noise on the fitting results.

© 2026 by the author(s). Distributed under a Creative Commons CC BY license.

Preprints.org (www.preprints.org) | NOT PEER-REVIEWED | Posted: 25 May 2026 doi:10.20944/preprints202605.1563.v1

To eliminate the high-frequency numerical oscillations introduced by the explicit dynamic solution and extract the quasi-static response trend, a piecewise smoothing and fitting method was applied to the original curve. The loading and unloading segments were fitted using cubic smoothing splines, with smoothing factors of $S_L = 3.50$ and $S_U = 1.89$, respectively. The peak-displacement region was smoothed using the Savitzky–Golay method, with a window length of 9 and a polynomial order of 2. The fitting accuracy was quantitatively evaluated using the coefficient of determination R^2 and the root mean square error (RMSE). The residual was defined as $e_i = y_i - \hat{y}_i$, and the coefficient of determination was calculated as

$$R^2 = 1 - \frac{\sum_{i=1}^{n}(y_i - \hat{y}_i)^2}{\sum_{i=1}^{n}(y_i - \bar{y}_i)^2} \tag{6}$$

The root mean square error was calculated as

$$RMSE = \sqrt{\frac{1}{n}\sum_{i=1}^{n}(y_i - \hat{y}_i)^2} \tag{7}$$

Where $\hat{y}_i$ is the fitted value, y_i is the original value, and $\bar{y}_i$ is the mean value of the original data.

Using Equations (6) and (7), the fitted curve was found to have $R^2 = 0.9938$ and $RMSE$ =1.98 N. The comparison between the simulated and fitted curves is shown in Figure 7. The two curves exhibit good agreement, indicating that the fitting results accurately capture the variation characteristics of the loading–unloading curve.

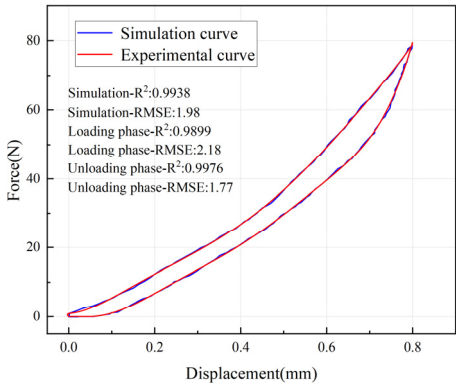

Figure 7. Comparison of simulation and fitted curve consistency.

Based on the force–displacement curve, the peak load and its corresponding displacement can be further extracted, and the average stiffness of the fuzz button during compression can be calculated [22]. The mechanical performance parameters of the mesoscopic fuzz button model are summarized in Table 6, where ΔW denotes the area enclosed by the hysteresis curve, U represents the maximum energy stored in the fuzz button during each cycle, η is the energy dissipation coefficient, and K_s is the average stiffness of the fuzz button.

Table 6. Mechanical properties of the meso-model of the fuzz button.

ΔW(N·mm)	U(N·mm)	η	K_s(N/mm)
5.1803	22.5002	0.07329	99.3793

© 2026 by the author(s). Distributed under a Creative Commons CC BY license.

Preprints.org (www.preprints.org) | NOT PEER-REVIEWED | Posted: 25 May 2026 doi:10.20944/preprints202605.1563.v1

4. Finite Element Simulation Validation

4.1. Experimental System and Testing Method

To validate the effectiveness of the established finite element simulation method, a typical compression condition was selected for comparative analysis between experimental testing and numerical simulation. The experimental specimens and finite element model were kept consistent in terms of geometric dimensions, material parameters, and loading displacement conditions to ensure the comparability of the results. A compression displacement amplitude of 0.20 mm was selected as the validation condition. The force–displacement curve, peak load, stiffness characteristics, and hysteresis behavior were used as the primary evaluation metrics for a comprehensive comparison between the simulation and experimental results. The detailed preparation process parameters of the fuzz button specimens are listed in Table 7.

Table 7. Specifications of the fuzz button.

Diameter (mm)	Height (mm)	Wire diameter (mm)	Filling ratio (%)	Porosity (%)
1.6	4	0.08	25	75

The comparison between experimental and simulation results enables validation of the rationality of the simulation method at both the macroscopic response and local feature levels. On the one hand, the overall mechanical curves of the fuzz button during the loading–unloading process were compared to verify the capability of the model to predict its nonlinear load-bearing behavior and rebound characteristics. On the other hand, the hysteresis area and residual deformation characteristics were analyzed to validate the ability of the model to characterize internal contact sliding and energy dissipation mechanisms.

The experiments were conducted using a self-developed quasi-static compression testing machine, as shown in Figure 8. The apparatus has a displacement resolution of 1.6 μm and a force resolution of 0.5 mN. The host-computer program provides functions for online recording, plotting, and data storage. The connection components were precision-machined from high-strength aluminum alloy and can satisfy the requirements for quasi-static compression testing of fuzz buttons with different dimensions within a small-deformation range.

During the experiment, the fuzz button specimen was placed between the upper and lower compression platens, and loading and unloading were performed under displacement control.

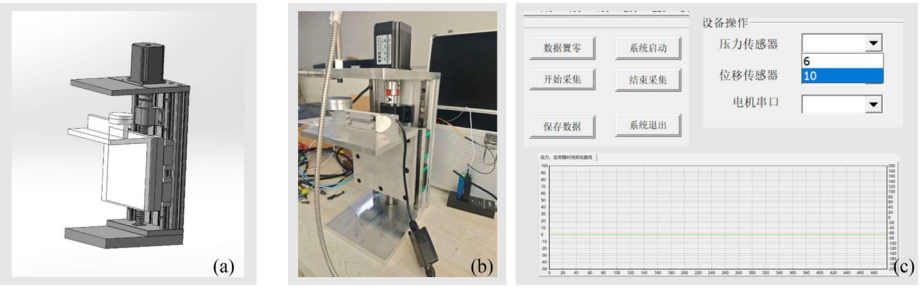

Figure 8. Fuzz button compression testing machine: (**a**) three-dimensional model; (**b**) physical photograph of the testing machine; (**c**) host-computer operating interface of the testing machine.

4.2. Comparative Analysis of Simulation and Experimental Results

To validate the accuracy of the finite element model, the compression condition with a displacement amplitude of 0.20 mm was selected for analysis. The simulated and experimental curves were plotted in the same coordinate system for comparison, as shown in Figure 9a. The coefficient of determination between the simulation and experimental data was $R^2 = 0.970$, indicating good agreement in the overall variation trend. During the compression loading stage, the fuzz button

© 2026 by the author(s). Distributed under a Creative Commons CC BY license.

Preprints.org (www.preprints.org) | NOT PEER-REVIEWED | Posted: 25 May 2026 doi:10.20944/preprints202605.1563.v1

exhibited a pronounced nonlinear stiffness-hardening behavior, whereas significant rebound occurred during unloading, forming a typical hysteresis curve. These results demonstrate that the established finite element model can accurately reproduce the fundamental mechanical response of the fuzz button under quasi-static compression conditions.

The comparison of peak loads shows that the simulated peak force was 79.36 N, slightly lower than the experimental peak force of 84.11 N, corresponding to a peak-load error of approximately 5.8%. This indicates that the model can effectively predict the load-bearing capacity of the fuzz button under a prescribed displacement condition. Further analysis of the curve slope variation shows that the simulation and experiment exhibit highly consistent trends in the initial loading stage, intermediate loading stage, and near the peak load, demonstrating that the model can effectively characterize the evolution of the compressive stiffness of the fuzz button.

The mechanical properties during the loading–unloading process were further extracted, as shown in in Figure 9b. The results show that the simulation and experiment are in good agreement in terms of hysteresis characteristics, with the errors of the four key variables (U, ΔW, η, and K_s) being less than or close to 10%, thereby satisfying engineering accuracy requirements. This indicates that the established model can effectively capture the macroscopic energy dissipation behavior caused by relative sliding and frictional energy dissipation among the internal metallic wires of the fuzz button, providing a reliable basis for subsequent design optimization and performance prediction.

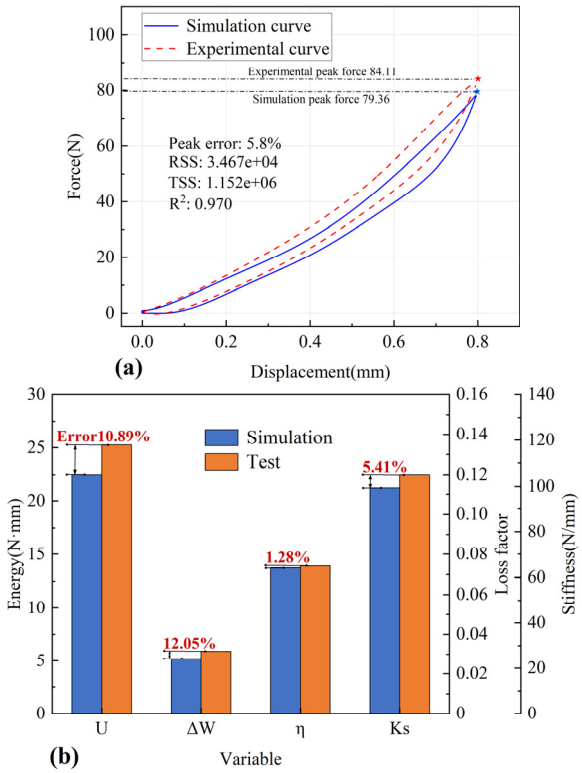

Figure 9. Comparison between numerical simulation and experimental results: (**a**) comparison of the simulated and experimental quasi-static loading–unloading processes; (**b**) comparison of the mechanical properties of the specimens obtained from numerical simulation and experiments.

Although the simulation and experimental results exhibit good agreement in key indicators, including the force–displacement response, peak load, stiffness evolution, and hysteresis characteristics, slight deviations remain between them. The main reasons are as follows: the winding configuration of metallic wires inside the real fuzz button exhibits pronounced randomness, and the virtual preparation model cannot fully reproduce the specific initial state and pre-contact conditions of each wire; the initial residual stress, local defects, and material property dispersion that may exist in the actual specimens were reasonably simplified in the model; and the adopted contact-related

© 2026 by the author(s). Distributed under a Creative Commons CC BY license.

Preprints.org (www.preprints.org) | NOT PEER-REVIEWED | Posted: 25 May 2026 doi:10.20944/preprints202605.1563.v1

parameters may also deviate slightly from their true values. The errors caused by these factors are within the acceptable range for engineering applications and do not affect the validity of the model or its subsequent application.

5. Conclusion

To address the complex mesostructure, pronounced contact nonlinearity, and difficulty in accurately characterizing the compressive mechanical behavior of fuzz button contacts, a mesoscopic finite element model of the fuzz button based on virtual fabrication was established in this study. The validity of the model was further verified by quasi-static compression experiments. The main conclusions are as follows:

1) A parametric method for generating the spatial trajectories of metallic wires was proposed based on the actual fabrication process and three-dimensional braiding concept. After trajectory smoothing and virtual compression forming in Abaqus, a mesoscopic finite element model with realistic geometrical morphology and internal contact topology was obtained.

2) A complete finite element simulation procedure was developed, including mesh generation, contact definition, analysis step configuration, boundary condition assignment, and post-processing. The model successfully reproduced the nonlinear stiffness enhancement and hysteretic energy dissipation behavior of the fuzz button during the loading–unloading process.

3) Under the validation condition with a compression displacement of 0.20 mm, the simulated peak load was 79.36 N, compared with the experimental value of 84.11 N, corresponding to a relative error of approximately 5.8%. The simulation and experimental results agreed well in terms of peak load, stiffness evolution, and hysteresis characteristics, with the errors of key mechanical indicators being less than or close to 10%. This demonstrates that the proposed model can accurately predict the compressive mechanical response of fuzz buttons and provide a reliable numerical basis for structural optimization and engineering applications.

Author Contributions: Conceptualization, X.D., Z.Z., M.H; methodology, M.H. and X.D.; software, M.H.; validation, M.H., Z.Z. and X.D.; formal analysis, Z.Z.; investigation, X.D.; resources, M.H.; data curation, Z.Z.; writing—original draft preparation, Z.Z.; writing—review and editing, H.M.; visualization, Z.Z.; supervision, X.D.; project administration, X.D.; funding acquisition, M.H. All authors have read and agreed to the published version of the manuscript.

Data Availability Statement: The processed data required to reproduce these findings cannot be shared at this time because the data also forms part of an ongoing research.

Conflicts of Interest: The authors declare no conflict of interest.

References

1. Chen, W.; Yang, D.; Chen, Z.; Fang, Y.; Zhong, L. Research on Degradation Law of Contact Performance for High-frequency Electrical Connectors in Long-term Storage Environment. *Journal of mechanical engineering* **2025**, *61*, 344-351.
2. Li, Q.; Li, J.; Chen, X.; Li, N.; She, Z.; Wang, L. The Overview and Research Status Analysis of Electrical Connectors. *Environmental Technology* **2021**, *39*, 115-119.
3. Ren, W.; Jiao, Y.; Zhai, G. Review of Fretting Wear for Electrical Connector. *Electromechanical Components* **2010**, *30*, 28-38.
4. Pan, J.; Jin, F.; Chen W.; Qian P. Structural Analysis of Electrical Connector Contacts and Insertion-Extraction Test. *China Mechanical Engineering* **2013**, *24*, 1636-1641.
5. Li, W.; Wang, J. Key technologies of miniaturization missile-borne guidance electronic equipments. *Journal of Terahertz Science and Electronic Information Technology* **2011**, *9*, 537-540.
6. Zhao, S.; Guan, D.; Zhu, J.; Su, Q.; Lin, J. Application of Composites in Lightweight Design of Airborne Electronic Equipment. *Plastics Science and Technology* **2025**, *53*, 214-219.

© 2026 by the author(s). Distributed under a Creative Commons CC BY license.

Preprints.org (www.preprints.org) | NOT PEER-REVIEWED | Posted: 25 May 2026 doi:10.20944/preprints202605.1563.v1

7. Hu, M.; Deng, C.; Li, C.; Li, D.; Li, S.; Shen, B.; Li, T.; Fan M. Thermal performance optimization of air-cooled electroni-c equipment arrangement under uniform and non-uniform heat flux conditions. *Applied Thermal Engineering* **2025**, *281*, 128646.
8. Puttlitz, K.; Galyon, G. Impact of the ROHS directive on high-performance electronic sy-stems-Part I: need for lead utilization in exempt systems. *Journal of Materials Science: Materials in Electronics* **2006**, *18*, 331-346.
9. Xu, L.; Wang. Z.; Hu, J.; Chen, Y.; Guo, Y. Vertical Interconnection Techniques for LTCC Microwave Modules on Basis of Fuzz-button. *Research & Progress of SSE* **2013**, *33*, 538-541.
10. Liu, X.; Hu, S.; Xiao, Q.; Deng, G.; Zheng, Y.; Gao, M.; Zhang, D.; Cao, H.; Wang, Z.; Chen, D.; Yang, W. An investigation of the electrical contact failure of JPT electric connectors used in automobiles under multiple stresses. *Wear* **2024**, *552*, 205458.
11. Harris, D.; Pecht, M. A reliability study of fuzz button interconnects. *Circuit World* **1995**, *21*, 12-18.
12. Lv, L.; Song, D.; Wang, X.; Xiao, S. The Effect of Materials Properties on the Spring-back Behavior and the Contact Resistance of Fuzz Button. *Electromechanical Components* **2021**, *41*, 41-46.
13. Huang, R.; Kong, Z.; Wang, B.; Zhang, L. Research on Mechanical Constitutive Model of Fuzz Button Connector. *Journal of Physics Conference Series* **2020**, *1626*, 012171.
14. Zhu, N.; Xiao, S. Research on Simulation Design of Buzz. *Electromechanical Components* **2025**, *45*, 11-12.
15. Zhang, Z.; Zhang, H.; Wang, B.; Zhang, L.; Zhu, M.; Yang, F.; Li, J. Electric Performance Model and Finite Element Analysis of Fuzz Button. *Journal of Physics: Conference Series.* **2020**, *1626*, 012005.
16. Lall, P.; Shinde, D.; Rickett, B.; Suhling, J. Finite Element Models for Simulation of Wear in Electrical Contacts. In 2008 11th Intersociety Conference on Thermal and Thermomechanical Phenomena in Electronic Systems, Proceedings of the 11th Intersociety Conference on Thermal and Thermomechanical Phenomena in Electronic Systems, Orlando, FL, USA, 28–31 May 2008; IEEE: New York, NY, USA, 2008; DOI: 10.1109/ITHERM.2008.4544353.
17. Zhu, Z.; Dong, X.; Huang, M.; Ren, Y. Simulation Research on Elastic Property of Wool Button Based on True 3D Model. *Computer Simulation* **2024**, *41*, 424-428.
18. Zhang, L.; Wang, S.; Tian, X.; Guo, J.; Mai, L. Research on Reliability Optimization of Fuzz Button Contacts. *Standard Science* **2025**, *S1*, 349-358.
19. Ma, L.; Wang, S.; Zhou, Q.; Yao, H. Summary of Products and Technical Level of Fuzz Button Contacts at Home and Abroad. *Standard Science* **2022**, *S1*, 254-259.
20. Shan, Z.; Zhou, Z.; Sun, Z.; Huang, H.; Liu, Y. Research of 3D Advanced Aerospace Composite Preforms Forming Technology and Equipment. *Journal of Mechanical Engineering* **2023**, *59*, 64-79.
21. Wang, W.; Gao, J.; Wang, Z.; Zhang, T.; Wang, C.; Bilal, H. Modeling and Analysis of Signal Integrity of High-Frequency Transmission Channel With Degraded Fuzz Button Connectors. *IEEE Transactions on Electromagnetic Compatibility* **2024**, *66*, 1888-1899.
22. Huang, R.; Zhang, Y.; Yang, F.; Liu, X. Research on the Key Technology of Standardization of Fuzz Button Contacts. Standard Science **2022**, *S1*, 214-218.
23. Wan, Z.; Jia, M.; Bao, W. Optimal configuration of embedded position and number of carbon nanotube yarns in 3-D braided composites. *Journal of Textile Research* **2021**, *42*, 76-82.
24. Ma, M.; Zhang, C.; Zhang, Y. Computer simulation of 3D four directional braided composites structure. *Journal of Tiangong University* **2019**, *38*, 45-51.
25. Xiao, L.; Kou, X.; Zuo, W. Study on the simulation of 3-D braided composites braiding process. *Computer Engineering & Science* **2014**, *36*, 719-724.
26. Zhang, Z.; Ma, X.; Wang, C.; Zheng, H.; Wang, L. A Geometrically Exact Curved Beam Element Based on Cubic Spline Interpolation. *Journal of Zhengzhou University(Engineering Science)* **2023**, *44*, 61-67.
27. Wu, S.; Li, Y.; Deng, C. Hermite Interpolation of Non-Uniform Cubic B-Spline Curve Based on PIA. *Chinese Journal of Computers* **2023**, *46*, 2463-2475.
28. Xu, M.; Liu, L. Blackman-harris window interpolated FFT algorithm based on cubic spline function. *Electric Power Automation Equipment* **2009**, *29*, 59-63.
29. Zheng, W.; Liang, Z.; Zhou, J.; Zhang, Y.; Jin, Z. Research on combined noise reduction of GNSS elevation data of paddy field grader with EMD and S-G filter. *Journal of South China Agricultural University* **2024**, *45*, 80-87.

© 2026 by the author(s). Distributed under a Creative Commons CC BY license.

Preprints.org (www.preprints.org) | NOT PEER-REVIEWED | Posted: 25 May 2026 doi:10.20944/preprints202605.1563.v1

30. Tubbs, A.; Ahmed, J.; Christopher, J.; Alvarez, J. Savitzky–Golay processing and bidimensional plotting of current–time signals from stochastic blocking electrochemistry to analyze mixtures of rod-shaped bacteria. *Analytical Methods* **2024**, *16*, 6570-6576.
31. Ding, L.; Yu, C.; Zhang,X.; Wen, Z.; Kan, Q.; Kang, G. Incremental strain gradient plasticity model and torsion simulation of copper micro-wires. *International Journal of Mechanical Sciences* **2023**, *239*, 107891.
32. Song, E.; Andani, M.; Misra, A. Investigation of grain size and geometrically necessary dislocation density dependence of flow stress in Mg-4Al by using nanoindentation. *Acta Materialia.* **2024**, *265*, 119633.
33. Bo, L.; Gao, X.; Song, W.; Ning, Z.; Sun, J.; Ngan, A.; Huang, Y. Size-dependent mechanical behaviors and mechanisms in CoCrFeNi microfibers. *International Journal of Plasticity* **2025**, *188*, 104307.
34. Wu, B.; Lu, C.; Liu, Z. Nanofabrication through forming: Techniques and mechanics. *Advances in Mechanics* **2022**, *52*, 153-179.
35. Kim, G.; Ni, J.; Koc, M. Modeling of the size effects on the behavior of metals in microscale deformation processes. *Journal of Manufacturing Science and Engineering* **2007**, *129*, 470-476.
36. Zhang, X.; Zhao, J.; Kang, G.;Zaiser, M. Geometrically necessary dislocations and related kinematic hardening in gradient grained materials: A nonlocal crystal plasticity study. *International Journal of Plasticity* **2023**, *163*, 103553.
37. Nix, W.; Gao, H. Indentation size effects in crystalline materials: A law for strain gradient plasticity. *Journal of the Mechanics and Physics of Solids* **1998**, *46*, 411-425.
38. Bellahkim, M.; Ouezgan, A.; Benbouras, Y.; Maziri, A.; Mallil, E.; Echaabi, J. 3D finite element analysis of laminated composites under three-point bending. *IOP Conference Series: Materials Science and Engineering* **2022**, *1244*, 012019.
39. Zhu, C. A finite element-mathematical programming method for elastoplastic contact problems with friction. *Finite Elements in Analysis and Design* **1995**, *20*, 273-282.
40. Moita, S.; Correia, F.; Soares, M. Influence of Applied Loads on Free Vibrations of Functionally Graded Material Plate–Shell Panels. *Applied Sciences* **2024**, *14*, 1993.
41. Wan, A.; Zhu, F.; Yun, X.; Li, D. Investigation on numerical analysis method of fatigue delamination damage of plane woven composites. *Acta Materiae Compositae Sinica* **2024**, *41*, 4418-4433.
42. Ivanyi, A.; Ivanyi, P.; Ivanyi, M.; Ivanyi, M. Hysteresis in structural dynamics. *Physica B: Condensed Matter* **2012**, *407*, 1412-1414.

Disclaimer/Publisher's Note: The statements, opinions and data contained in all publications are solely those of the individual author(s) and contributor(s) and not of MDPI and/or the editor(s). MDPI and/or the editor(s) disclaim responsibility for any injury to people or property resulting from any ideas, methods, instructions or products referred to in the content.

© 2026 by the author(s). Distributed under a Creative Commons CC BY license.